Available online at www.sciencedirect.com

ScienceDirect

Physics Procedia 54 (2014) 2 – 9

Physics Procedia

International Conference on Magnetic Materials and Applications, MagMA 2013

Magnetic properties of $Zn_{1-x}Co_xO$ nanoparticles.

Ningthoujam Surajkumar Singh[a,b,*], Shougaijam Dorendrajit Singh[b], Sujit Kumar Bandyopadhyay[c]

[a]*Department of Physics, Pachhunga University College, Aizawl,Mizoram – 796001, India*
[b]*Department of Physics, Manipur University, Canchipur, Manipur -795003, India,* [c]*VEC Centre, I/AF, Bidhan Nagar, Kolkata -700064, India*

Abstract

$Zn_{1-x}Co_xO$ nanoparticles have been synthesized at various concentrations of Co^{2+} doping ($0.005 \leq x \geq 0.15$) by wet chemical method. Particle size was ranging from 34 – 45 nm. The magnetic moment increases from x = 0.005 and 0.01 sample to x = 0.04 sample drastically showing a value of magnetic moment as high as 8.54 μ_B/Cations and then decreases for x = 0.09 and 0.15 values of Co^{2+} doping. There is almost paramagnetic behaviour for x = 0.005 and 0.01 Co^{2+} doped samples. The x = 0.04 sample shows ferromagnetic ordering. Ferromagnetic behaviour decreases for x = 0.09 and 0.15 samples as the antiferromagnetic interaction dominates at higher Co^{2+} doping concentrations. To probe the source of magnetism, we have undertaken photoluminescence studies also which revealed the presence of oxygen and Zinc vacancies along with other defects.

Peer-review under responsibility of Department of Physics, Indian Institute of Technology Guwahati

Keywords: ZnO:Co; nanoparticles; dilute magnetic semiconductors; ferromagnetic; photoluminescence

1. Introduction

Diluted magnetic semiconductors are the most puzzling and intriguing in understanding. Since Dietl [1] proposed the idea of ferromagnetism introduced in the semiconductors by the presence of magnetic cations like Manganese (Mn) doped in semiconductor matrix, there has been a flood of reports of these doped semiconductors [1-9]. Diluted magnetic semiconductors (DMSs) formed by substituting the cations of III – V or II – VI nonmagnetic semiconductors by ferromagnetic Mn, Fe, Co and Ni exhibit a number of unique, magneto-optical and magneto-transport pro-

* Corresponding author. Tel.: +919616354237; fax: +91-389-231-5212.
E-mail address: surajningthoujam@yahoo.co.in

Peer-review under responsibility of Department of Physics, Indian Institute of Technology Guwahati
doi:10.1016/j.phpro.2014.10.029

perties, pertinent for magneto-electronic and spintronic devices [2,7]. Room temperature [RT] ferromagnetism (FM) in transition metal (TM) doped zinc oxide (ZnO) has been continually envisaged by numerous groups using variety of calculations/simulation studies [1, 4]. ZnO-based diluted magnetic semiconductors have been predicted to have ferromagnetic properties with Curie temperature (T_C) above room temperature [1, 5, and 6]. Rath *et al.* [7] also studied the magnetic property of ZnO:Co nanoparticles and reported that the material exhibits paramagnetic behaviour. Rao *et al.* [8] investigated the structural, optical and electrical properties of ZnO thin films prepared by spray pyrolysis technique. ZnO, which is a direct band gap semiconductor with a band gap of 3.37 eV having an excitonic binding energy of 60 meV [8], because of its potential applications, makes one of the most encouraging materials for probable applications in spintronics and as diluted magnetic semiconductor (DMSs) material. Although much experimental research has been focused in this area, the origin of ferromagnetism in DMS materials is still under debate [10].

There have been reports of exceedingly high magnetic moments per impurity atoms in dilute magnetic semiconductors. A "Giant magnetic moments" of 22.9 Bohr magneton (μ_B) per impurity atom has been found for TiO_2 doped with Co [11]. A high value of magnetic moment equal to 18.9 μ_B per impurity atom was reported for Co doped ZnO films [12]. The magnetic moment values of 2.6 μ_B [11], 3.66-3.87 μ_B [7], 7.5 μ_B [13] and 8.2 μ_B [14] were found correspondingly, for semiconducting materials ZnO, SnO_2 and CeO_2 doped with Co.

In the present paper, we divulge a simple technique to synthesize $Zn_{1-x}Co_xO$ nanoparticles with excellent magnetic properties. X-ray diffraction (XRD), energy-dispersive analysis of X-ray (EDAX), transmission electron microscope (TEM), vibrating sample magnetometer (VSM) for magnetic properties and photoluminescence (PL) studies on $Zn_{1-x}Co_xO$ nanoparticles (with x = 0.005, 0.01, 0.04, 0.09and 0.15) synthesized by Wet Chemical method having particle sizes of 34-45 nm are reported in this paper. XRD shows that Co^{2+} ions were incorporated well into ZnO lattice. Only the x = 0.15 sample shows the presence of small amount of Co_3O_4 phases. We found that system changes from paramagnetism at (x = 0.005 and x = 0.01) to ferromagnetism at (x = 0.04) and showing a magnetic moment value as high as 8.54 μ_B per cations and then towards antiferromagnetic interaction at x values higher than 0.04.

Many possible mechanisms such as Ruderman-Kittel-Kasuya-Yosida (RKKY) [15, 16], double-exchange mechanism [17, 18], and percolation of bound magnetic polarons (BMPs) have been proposed [19]. The PL spectra show the presence of defects. These defects, magnetic cations and carriers made up BMPs. Thus ferromagnetism can be understood within the framework of percolation of bound magnetic polarons.

2. Experimental methods

2gms of Zinc chloride (Sigma-Aldrich 99.99% purity) and appropriate amount of Cobalt acetate (Sigma-Aldrich 99.999% purity) to make the desire doping percentage was dissolved in 50ml distilled water. 150ml Ethylene glycol was added to the above solution. 6gm Urea was then added to the above solution. The solution was heated on a round bottom flask fitted with condenser and the temperature was maintained at 140°C for 2 hours. The precipitates formed were collected by centrifugation after washing with Methanol and finally with distilled water. The precipitates were dried at around 80°C to 100°C for 24 hours. In our experiment six samples were prepared at different doping percentages of Cobalt. The Cobalt atomic percentages taken were 0% (undoped), 0.5%, 1%, 4%, 9% and 15%. The dried precipitates of all the samples of $Zn_{1-x}Co_xO$ nanoparticles (x = 0, 0.005, 0.01, 0.04, 0.09 and 0.15 to make the corresponding atomic percentages of Co doping) so prepared were finally annealed at 500°C for 2 hours.

XRD of the samples were carried out using Bruker-Nonius FR-590, MACH-3, Single Crystal X-Ray Diffractometer. The XRD lines were identified with the Joint Committee on Powder Diffraction Standards (JCPDS) standard data files. Compositions of the synthesized nanoparticles were quantified by energy-dispersive analysis of X-ray (EDAX) using energy-dispersive X-ray (EDX) spectrometer attached to scanning electron microscope (SEM), FEI Quanta 250. TEM micrographs were taken using a PHILIPS make CM200 model Transmission Electron Microscope. Samples were dispersed in methanol by sonication and placed on the copper grid for this purpose. Magnetic properties measurements were carried out using Vibrating Sample Magnetometer (VSM), Lakeshore Model no. 7407 for the M-H at three different temperatures, viz. 80 K, 150 K and 300 K for up to 1.5 Tesla field. Photoluminescence measurements were also done using Perkin Elmer LS-55 Luminescence Spectrometer.

3. Results and discussions

3.1. X-Ray diffraction

Figure 1 shows the XRD pattern of the $Zn_{1-x}Co_xO$ nanoparticles synthesize in the present work. XRD spectra show peaks at positions which are in agreement with the standard JCPDS file for ZnO (JCPDS 36 – 1451, $a = b = 3.249$Å, $c = 5.206$Å) and can be indexed as the hexagonal wurtzite structure of ZnO having space group $P6_{3mc}$ [20]. With increasing concen-tration of cobalt doping in the samples, the spectra remain the same with decrease in XRD intensity, indicating that Co ions successfully substituting the Zn sites in the wurtzite structure. Only for the sample with x = 0.15, there are some small peaks corresponding to Co_3O_4 [21]. The almost same crystallite size, stable wurtzite structure and absence of impurity phases with increasing concentration of Co^{2+} doping for all samples could be attributed to the similarity of size of Zn^{2+} and Co^{2+} ions (ionic radius of Co^{2+} is 0.59Å, Zn^{2+} is 0.60Å) [20] .

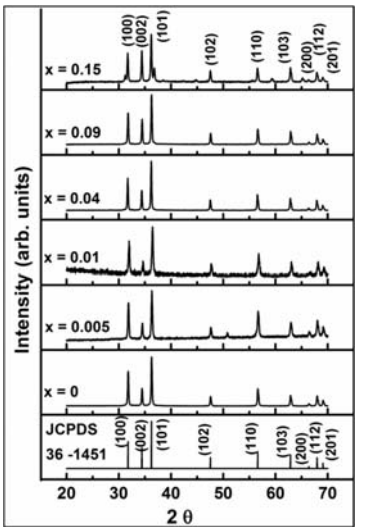

Figure 1. XRD spectra of $Zn_{1-x}Co_xO$ nanoparticles at different x values.

The crystallite size, d, of $Zn_{1-x}Co_xO$ nanoparticles were estimated by Scherrer's formula [20, 22]:

$$d = \frac{0.9\lambda}{B\cos\theta} \qquad (1)$$

where d is the crystallite size; λ is the wavelength of radiation used; θ is the Bragg angle and B is the full width at half maxima (FWHM); for spherically shaped crystals/particles, 0.9 is normally taken as the value of constant k [23, 24]. The crystallite sizes were estimated from the first three most prominent X-ray diffractions; corresponding to (101), (002) and (100) peaks and then mean values was calculated from those three values. The sizes of the nanoparticles were found to be in 34 - 45 nm range for different samples.

3.2. Energy dispersive X-ray analysis

EDAX measurements were performed, in order to confirm the presence of Co^{2+} in the synthesized $Zn_{1-x}Co_xO$ nanoparticles and to determine their compositions. EDAX spectra displayed in figure 2 demonstrate the presence of various elements in the prepared doped samples. The EDAX analysis provided precise composition of the elements. The EDAX spectra in figure 2 (a), (b), (c), (d), (e) and (f) show peaks corresponding to elements Zn, O and Co for samples with x values corresponding to 0, 0.5, 1, 4, 9 and 15 atomic percentage of Co^{2+} doping concentrations

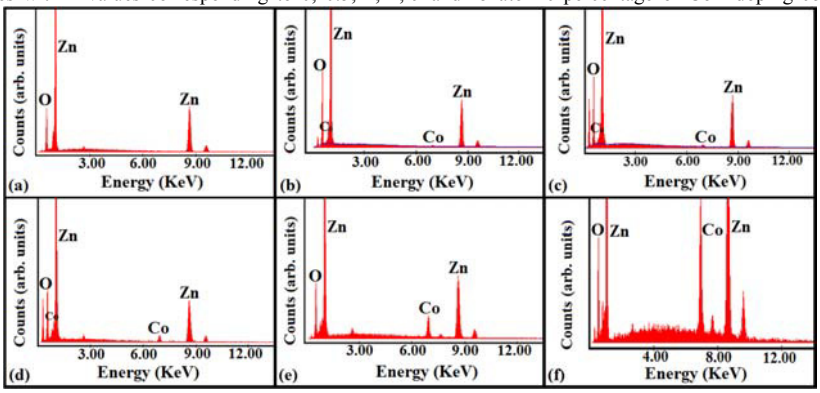

Figure 2. EDAX spectra of $Zn_{1-x}Co_xO$ for (a) x = 0, (b) x = 0.005, (c) x = 0.01, (d) x = 0.04, x = 0.09 and (d) x = 0.15.

respectively.

3.3. Transmission Electron Microscopy

Figure 3 (a) shows the representative TEM image of the x=0.09 sample. The histogram is being given in figure 3 (b). The mean particle size is found to be 45nm in agreement with that obtained from XRD.

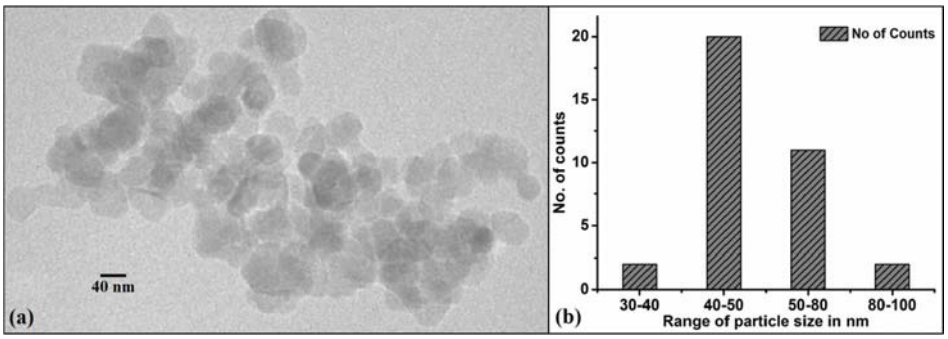

Figure 3. (a) Representative TEM micrograph of x = 0.09 sample. **(b)** Histogram for x = 0.09 sample giving average size of 45 nm.

3.4. Magnetic Properties

The magnetic properties of the $Zn_{1-x}Co_xO$ (x = 0.005, 0.01, 0.04, 0.09, 0.15) at three temperature values of 80 K, 150 K and 300 K are shown in figure 4. In all the samples the magnetization does not approach saturation even at 1.5 Tesla. The M-H curves are linear in case of x = 0.005 and 0.01 samples showing paramagnetic behaviours.

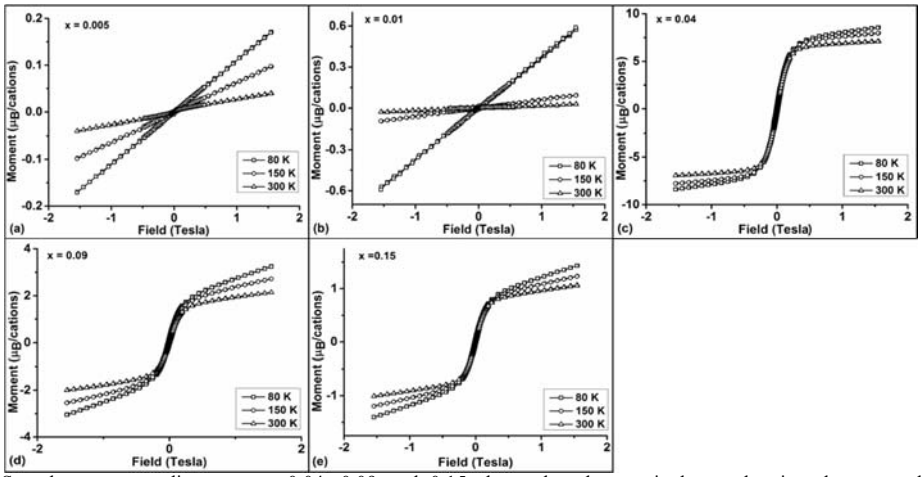

Figure 4. M-H plots for $Zn_{1-x}Co_xO$ at 80 K, 150 K and 300 k for **(a).** x = 0.005, **(b).** x = 0.01, **(c).** x = 0.04, **(d).** x = 0.09 and **(e).** x = 0.15

ferromagnetic and the corresponding values of Coercivity field (H_C) and Remanence magnetization (R_m) are given in table 1 (a). At 80 K the x = 0.4 sample has value of R_m equal to 0.32 μ_B /cations and the x = 0.15 sample has this value equal to 0.04 μ_B /cations.

Table 1. (a) Remanence magnetization (R_m) and Coercivity field (H_C) for x = 0.07, 0.09 and 0.2 samples of $Zn_{1-x}Co_xO$.

Temp.	x = 0.04		x = 0.09		x = 0.15	
	R_m (μ_B /cations)	H_C (Tesla)	R_m (μ_B /cations)	H_C (Tesla)	R_m (μ_B /cations)	H_C (Tesla)
80 K	0.32	0.007	0.09	0.008	0.04	0.007
150 K	0.26	0.006	0.08	0.008	0.04	0.008
300 K	0.20	0.006	0.06	0.007	0.03	0.006

This decrease shows ferromagnetism decreases as the Co^{2+} doping concentration increases from x = 0.04. Figure 5 shows the hysteresis loops of sample corresponding to x = 0.04, x = 0.09 and x = 0.15 sample at 80 K at low field range.

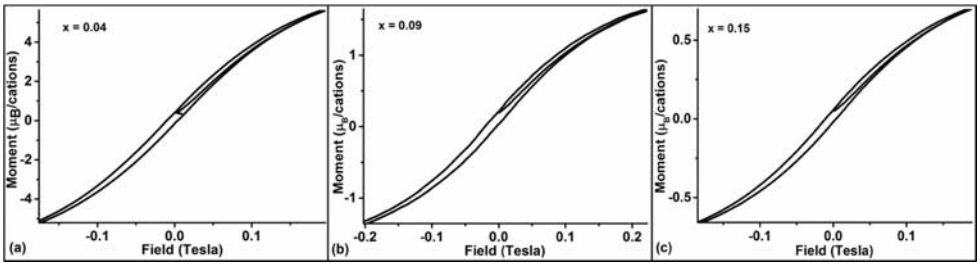

Figure 5. Hysteresis loop at low field range at 80 K for **(a)** x = 0.04, (b) x = 0.09 and (c) x = 0.15

Table 1 (b) shows the value of moment of the samples at 1.5 Tesla field in μ_B /cations units. The values of moment increases from x = 0.005 sample to x = 0.04 sample then shows decreasing trend for higher values of x. The x=0.04 sample shows highest value of moment per cation, a value equal to 8.54 μ_B per cations. Thus the VSM measurements show an evolution from paramagnetic to ferromagnetism and then to antiferromagnetism depending on the Co^{2+} doping concentrations.

Table 1. (b) Moment of $Zn_{1-x}Co_xO$ in (μ_B /cations) at 1.5 Tesla for different x values and at three temperature (Temp.) values.

Moment (μ_B /cations) at different x values and temperatures					
Temp.	x = 0.005	x = 0.01	x = 0.04	x = 0.09	x = 0.15
80 K	0.31	0.58	8.54	3.25	1.43
150 K	0.16	0.09	7.94	2.72	1.23
300 K	0.02	0.03	7.09	2.14	1.06

To explain this phenomenon, we have to understand the origin of this magnetism. There are several mechanisms for the origin of this ferromagnetism in DMSs. The RKKY interaction is based on free electrons, but ZnO cannot transform into a metal at low doping. Direct interactions such as double-exchange cannot be responsible for the ferromagnetism at low doping of magnetic cations [10]. One origin which is due to the small secondary phases of Co can also be ruled out except in case of x = 0.15 sample as the XRD of other samples show no secondary phases. Scharwtz and Gamelin [25] reported that the room-temperature ferromagnetic ordering in Co^{2+} doped ZnO could be switched between ‘on’ and ‘off’ when introducing or removing defects of ZnO. The increasing dependence of

ferromagnetic ordering on Co^{2+} content was observed [26]. According to literature [10, 19], magnetic cations, carriers and defects can make up bound magnetic polarons (BMPs). For semiconductors with low carrier densities such as oxides, the magnetic polaron mechanism is applicable [27, 28]. In this model, the spins of magnetic dopants incorporated into the semiconductor lattice interact through a donor-impurity band, formed by lattice defects such as oxygen vacancies (V_o) [22]. Coey *et al.* [19] explain the spin-alignment of the 3d transition-metal cations by coupling of their spins, which are antiparallel to the spin of donor electrons residing in hydrogenic orbits. Due to this coupling, all spins within this expanded orbit are aligned. Because of the overlap of different orbits, an impurity band is formed, aligning a huge number of 3d magnetic spins parallel, resulting in ferromagnetism. In the framework of this theory, not only the dopant concentration but also the number of donor electrons must be quite large in order to obtain ferromagnetism. Nanoparticles possess a lot of such defect sites because of their comparatively large surface, which, naturally, has many defects in the form of unsaturated bonds [27]. Rubi *et al.* demonstrated that magnetism of Co-doped ZnO powders can be switched reversibly from ferro- to paramagnetic behaviour by annealing in either oxygen-poor or oxygen-rich atmosphere, resulting in the generation or cancellation of V_o, respectively [29]. Contrary to small particles, bulk single crystals of ZnO:Co, grown at near-equilibrium, exhibits a very low defect concentration and show no ferromagnetism but behave para-magnetically [30]. These observations strengthen the concept of an impurity-band exchange by magnetic polarons evoked by V_o in the ZnO:Co nanoparticles. The magnetic phase diagram evolves from para at lower polaron concentration to ferromagnetic ordering at concentration below percolation threshold and then to antiferromagnetic ordering beyond the percolation threshold [19]. In low doping samples, the BMPs are isolated so that paramagnetic interaction is observed. More doping produces more BMPs, leading to the overlap of BMPs at which point the ferromagnetic interaction becomes long-range [10]. There is distinct dependency on the maximum attainable magnetization of $Zn_{1-x}Co_xO$ samples on the Co^{2+} doping percentage [27]. From these theoretical and experimental results, it becomes evident that not only the dopant concentration but also the amount of defect sites has to be substantial enough to get a ferromagnetic coupling of the magnetic spins. In the framework of the polaron model, the defect concentration has to exceed the polaron percolation threshold [27].

In our case magnetism evolves from paramagnetic at x = 0.005 and x = 0.01 to ferromagnetic at x = 0.04 as the BMPs are about to percolate and then to antiferromagnetic interaction as the doping concentration goes up beyond x = 0.04. Above x = 0.04 the magnetic moment decreases with dopant concentration. This behaviour can be explained by the fact that for high concentrations it is more probable for dopant atoms to occupy next-nearest lattice sites. Such Co^{2+} pairs couple by super-exchange over the intermediate oxygen atom in an antiferromagnetic way. The enhanced antiferromagnetic interaction between neighbouring Co^{2+}- Co^{2+} ions suppressed the ferromagnetism at higher doping concentration of Co^{2+} [3].

3.5. Photoluminescence

The room temperature photoluminescence spectra of $Zn_{1-x}Co_xO$ nanoparticle samples are shown in figure 6. The spectra were recorded with excitation at 325 nm radiation for detecting PL peaks in the range 350 - 600 nm. The sample with x = 0.005 exhibits three peaks centred around 390 nm, 420 nm and 438 nm and two other weaker peaks at 480 nm and 508 nm. The fluorescence at 390nm corresponds to the characteristic band edge emission [9]. The peak at 420nm corresponds to the transitions from Co^{2+} ions substituting Zn^{2+} ions [31]. The violet luminescence at 438nm has been assigned to transitions from Zn_i level to valence band [9]. The weak emissions at 480 nm and 508 nm correspond to Zn-vacancy (V_{Zn}) and O-vacancy (V_O) respectively [32]. Emissions in the range 381- 389 nm are originated from excitonic recombination corresponding to near band edge (NBE) exciton emission of wide band gap ZnO [33]. As the doping concentration increases the intensity of the UV emission peaks decreases successively and the UV peak position shifts to lower wavelength. The weak defect emissions become prominent at higher Co^{2+} doping if we consider the relative decrease in

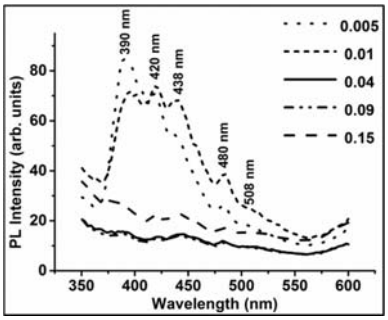

Figure 6. PL spectra for $Zn_{1-x}Co_xO$ at different x values with excitation wavelength of 325 nm and emission range 350-600 nm.

intensities. More defect states below the conduction band occurred by Co^{2+} doping, so that some of the excited electrons in the conduction band relax to the defect states, leading to decrease in UV emission intensity [31, 34, 35]. So we conclude that PL confirms the presence of defects which are the constituents of the BMPs.

4. Conclusion

We have successfully synthesized diluted magnetic semiconductor $Zn_{1-x}Co_xO$ nanoparticles of average size 34 – 45 nm by wet chemical synthesis. The XRD spectra demonstrated substitution of Co^{2+} cations to the Zn^{2+} sites in the ZnO wurtzite structure. Photoluminescence shows the presence of various defects and doped impurities. Initially these nanoparticles at low Co^{2+} concentrations show paramagnetic behaviour. At x = 0.04 the ferromagnetic behaviour is most prominent. However at higher doping percentage of Co^{2+} the ferromagnetic behaviour was suppressed and antiferromagnetic nature was enhanced. This evolution from paramagnetic behaviour to ferromagnetic behaviour depending on the doping concentration and then to antiferromagnetic behaviour in $Zn_{1-x}Co_xO$ nanoparticles systems can be understood within the framework of percolation of bound magnetic polarons.

Acknowledgments

One of the authors (Ningthoujam Surajkumar Singh) gratefully acknowledges UGC for financial support under minor research project to carry out this research work.

References

[1] Dietl T, Ohno H, Matsukura F, Cibert J, Ferrand D. Zener model description of ferromagnetism in zinc-blende magnetic semiconductors. *Science* 2000; 287: 1019.
[2] Pan Q, Huang K, Ni S, Yang F, Lin S, and He D. Photoluminescence and magnetism in Co-doped ZnO powder. *J Phys D: Appl Phys* 2007; 40: 6829.
[3] Goshal S, Anil Kumar P S. Process-dependent magnetic properties of Co-doped ZnO in bulk and thin film form. *J Mag Mag Mat* 2008; 320: L93.
[4] Sluiter M H F, Kawazoe Y, Sharma P, Inoue A, Raju A R, Rout C, Waghmare U V. First principles based design and experimental evidence for a ZnO-based ferromagnet at room temperature. *Phys Rev Lett* 2005; 94: 187204.
[5] Sundaresan A, Bhargavi R, Rangarajan N, Siddesh U, Rao C N R. Ferromagnetism as a universal feature of nanoparticles of the otherwise nonmagnetic oxides. *Phy Rev B* 2006; 74: 161306(R).
[6] Sundaresan A, Rao C N R. Ferromagnetism as a universal feature of inorganic nanoparticles. *Nano Today* 2009; 4: 96.
[7] Rath C, Singh S, Mallick P, Pandey D, Lalla N P, Mishra N C. Effect of cobalt substitution on microstructure and magnetic properties in ZnO nanoparticles. *Ind J Phys* 2009; 83: 415.
[8] Rao T P, Kumar M C S, Ganesan V. Effect of annealing on the structural, optical and electrical properties of ZnO thin films by spray pyrolysis. *Ind J Phys* 2011; 85: 1381.
[9] Mallick P, Rath C, Biswal R, Mishra N C. Structural and magnetic properties of Fe doped NiO. *Ind J Phys* 2009; 83: 517.
[10] Zou Y, Qu Z, Fang J, Zhang Y. Intrinsic magnetism of $Zn_{1-x}Co_xO$ single-crystalline nanorods prepared by solvothermal method. *J Mag Mag Mat* 2009; 321: 3352.
[11] Orlov A F, Balagurov L A, Konstantinova A S, Perov N S, Yarkin D G. Giant magnetic moments in dilute magnetic semiconductors. *J Mag Mag Mat* 2008; 320: 895.
[12] Zukova A, Teiserskis A, VanDijken S, Gun'ko Y K, Kazlauskiene V. Giant moment and magnetic anisotropy in Co-doped ZnO films grown by pulse-injection metal organic chemical vapour deposition. *Appl Phys Lett* 2006; 89: 232503.
[13] Ogale S B, Choudhary R J, Budan J P. High temperature ferromagnetism with a giant magnetic moment in transparent Co-doped SnO_2. *Phys Rev Lett* 2003; 91: 077205.
[14] Tiwari A, Bhosle V M, Ramachandran S. Ferromagnetism in Co doped: Observation of a giant magnetic moment with a high Curie temperature. *Appl Phys Lett* 2006; 88: 142511.
[15] Dietl T, Ohno H, Matsukura F. Hole-mediated ferromagnetism in tetrahedrally coordinated semiconductors. *Phys Rev B* 2001; 63: 195205.
[16] Jalbout A F, Chen H, Whittenberg S L. Monte Carlo simulation on the indirect exchange interactions of Co-doped ZnO film. *Appl Phy Lett* 2002; 81: 2217.
[17] Koshihara S, Oiwa A, Hirasawa M, Katsumoto S, Iye Y, Urano C, Takagi H, Munekata H. Ferromagnetic order induced by photogenerated carriers in magnetic III-V semiconductor heterostructures of (In, Mn)As/GaSb. *Phys Rev Lett* 1997; 78: 4617.
[18] Sato K, Yoshida H K. Material design for transparent ferromagnets with ZnO-based magnetic semiconductors. *Jpn J Appl Phys* 2000; 39: L555.
[19] Coey J M D, Venkatesan M, Fitzgerald C B. Donor impurity band exchange in dilute ferromagnetic oxides. *Nature Mater* 2005; 4: 173.
[20] Sharma P K, Dutta R K, Pandey A C. Alteration of magnetic and optical properties of ultrafine dilute magnetic semiconductor ZnO:Co^{2+} nanoparticles. *J Coll Int Sc* 2010; 345: 149.
[21] Sharma V K, Varma G D. Co nanoclusters as origin of ferromagnetism in sol-gel synthesized $Zn_{1-x}Co_xO$ (x = 0.05, 0.10 and 0.15) samples. *Cryst Res Technol* 2008; 43: 1046.
[22] Khranovskyy V, Grossner U, Nilson O, Lazorenko V, Lashkarev G V, Svensson B G, Ykimova R. Structural and morphological properties

of ZnO:Ga thin films. *Thin Solid Films* 2006; 515: 472.
[23] Langford J L, and Wilson A J C. Scherrer after sixty years: A survey and some results in the determination of crystallite size. *J Appl Cryst* 1978; 11: 102-113.
[24] Ahmad M, Mohammad R F, Mohammad R M. Modified Scherrer equation to estimate more accurately nano-crystallite size using XRD. *World Journal of Nano Science and Engineering* 2012; 2: 154-160.
[25] Schwartz D A, Gamelin D R. Reversible 300 K ferromagnetic ordering in a diluted magnetic semiconductor. *Adv Mater* 2004; 16: 2115.
[26] Xu X, Cao C. Structure and ferromagnetic properties of Co-doped ZnO powders. *J Mag Mag M*at 2009; 321: 2216.
[27] Büsgen T, Hilgendroff M, Irsen S, Wilhelm F, Rogalev A, Goll D, Giersig M. Colloidal cobalt-doped ZnO nanorods: synthesis, structural and magnetic properties. *J Phys Chem C* 2008; 112: 2412.
[28] Pearton S J, Heo W H, Ivil M, Norton D P, Steiner T. Dilute magnetic semiconducting oxides. *Semicond Sci Technol* 2004; 19: R59.
[29] Rubi D, Fontcuberta J, Calleja A, Aragones L, Capdevila X G, Segarra M. Reversible ferromagnetic switching in ZnO:(Co, Mn) powders. *Phys Rev B* 2007; 75: 155322.
[30] Kane M H. Magnetic and optical properties of single crystals of transition metal doped ZnO. *Phys Status Solidi B* 2007; 244: 1462.
[31] Wang A, Zhang B, Wang X, Yao N, Gao Z, Ma Y, Zhang L, Ma H. Nano-structure, magnetic and optical properties of Co-doped ZnO films prepared by a wet chemical method. *J Phys D: Appl.Phys* 2008; 41: 215308.
[32] Yang L L, Zhao Q X, Willander M, Yang J H, Ivanov I. Annealing effects on optical properties of low temperature grown ZnO nanorod arrays. *J Appl Phys* 2009; 105: 053503.
[33] Pearton S J, Abernathy C R, Overberg M E, Thater G T, Norton D P, Theodoropoulou N, Hebord A F, Park Y D, Ren F, Kin J, Boatner L A. Wide band gap ferromagnetic semiconductors and oxides. *J Appl Phys* 2003; 93: 1.
[34] Maensiri S, Laokul P, Promarak V. Synthesis and optical properties of nanocrystalline ZnO powders by a simple method using zinc acetate dihydrate and polyvinyl pyrrolidone. *J Cryst Growth* 2006; 289: 102.
[35] Liu C, Yun F, Morkoc H. Ferromagnetism of ZnO and GaN: A Review. *J Mater Science: Materials in Electronics review* 2005; 16: 555.